Title	Single step synthesis of Ge-SiOx core-shell heterostructured nanowires
Authors	Arnold, Donna C.;Hobbs, Richard G.;Zirngast, Michaela;Marschner, Christoph;Hill, Justin J.;Ziegler, Kirk J.;Morris, Michael A.;Holmes, Justin D.
Publication date	2009-01-06
Original Citation	Arnold, D. C., Hobbs, R. G., Zirngast, M., Marschner, C., Hill, J. J., Ziegler, K. J., Morris, M. A. and Holmes, J. D. (2009) 'Single step synthesis of Ge–SiOx core-shell heterostructured nanowires', Journal of Materials Chemistry, 19(7), pp. 954-961. doi: 10.1039/B816727C
Type of publication	Article (peer-reviewed)
Link to publisher's version	10.1039/B816727C
Rights	© The Royal Society of Chemistry 2009
Download date	2024-04-19 22:45:03
Item downloaded from	https://hdl.handle.net/10468/8156

ARTICLE TYPE www.rsc.org/xxxxxx | XXXXXXXX

Single Step Synthesis of Ge-SiO_x Core-Shell Heterostructured Nanowires

Donna C. Arnold,[a] Richard G. Hobbs,[a] Michaela Zirngast,[b] Christoph Marschner,[b] Justin J. Hill,[c] Kirk J. Ziegler,[c] Michael A. Morris[a] and Justin D. Holmes*[a]

Received (in XXX, XXX) Xth XXXXXXXXX 200X, Accepted Xth XXXXXXXXX 200X
First published on the web Xth XXXXXXXXX 200X
DOI: 10.1039/b000000x

The ability to control the morphology of heterostructured nanowires, through the design of precursors and by careful manipulation of reaction parameters, is important if these materials are to be utilised as components in future nanodevices. Traditionally core-shell heterostructured nanowires have been synthesised through multi-precursor and/or multi-step synthetic routes. In this paper we discuss the synthesis of core-shell, Ge-SiO_x heterostructured nanowires using a single source precursor and a single step supercritical fluid reaction process.

Introduction

Recently extensive research has been conducted into the synthesis of core–shell nanoparticles and nanowires primarily because, in principle, their physical and chemical properties can be tuned by controlling their chemical composition and the relative sizes of the core and shell.[1] The synthesis of one-dimensional nanowire or nanocable heterostructures consisting of a crystalline wire encapsulated in a sheath of a different material are of particular interest as they are potentially new materials for spintronic devices,[2-5] light-emitting diode applications[6] and field effect transisitors (FET).[7]

The continued drive towards miniaturisation of the semiconductor industry in accordance with Moore's Law has led to renewed interest in germanium. The reasons for this are twofold. Firstly, germanium possesses superior charge carrier transport properties relative to silicon, due to the lower effective masses of electrons and holes within the cubic germanium lattice. Secondly, germanium exhibits quantum confinement effects at larger dimensions than silicon because of its larger excitonic Bohr radius.[8, 9] However, in contrast with silicon, the native germanium oxide is not stable and is soluble in water limiting its usefulness.[9] In addition the Ge/GeO_2 interface has a higher trap/surface state density than the Si/SiO_2 interface.[9] The synthesis of core/shell nanowires or the addition of passivation layers to the germanium may offer a solution to these interface problems. In particular core/shell nanowires based on germanium have attracted much attention owing to their low temperature synthesis, high bulk mobility and compatibility with conventional CMOS technology with an active area of research being the continued optimisation of single nanowire FETs.[10, 11] The synthesis of heterostructured nanowires based solely on semiconductor materials has been reported by Lieber *et al* who pioneered the development of semiconductor Ge-Si core-shell heterostructured nanowires.[2] These nanowires were formed by chemical vapour deposition (CVD) whereby first the Ge precursor was decomposed to form the Ge core nanowires. The precursor and reaction conditions were then changed and the Si sheath formed around the Ge nanowires. They further found that it was possible to completely crystallise the amorphous Si shell through in-situ annealing at 600 ^oC provided no GeO_2 formed at the core-shell interface, with no evidence of Si-Ge inter-diffusion.[2] Other authors have reported Si/$Si_{1-x}Ge_x$ core/shell nanowires grown by MBE methods and Ge-$Si_{1-x}Ge_xO_y$ and GeO_2-$Si_{1-x}Ge_xO_y$ core-shell nanowires using a high temperature carbothermal method.[12-14] More recently Lieber and co-workers have shown the possibility of using these materials as field effect transistors which demonstrated high performance device characteristics.[10, 15] Xiang and co-workers have also proposed that Ge/Si core/shell heterostructures are ideal for investigating the interplay between 1 D quantum confinement and superconductivity.[16] These materials displayed tuneable dissipationless supercurrents as well as clear signatures of multiple Andreev reflections and demonstrate the synthesis of mesoscopic Josephson junctions. More complex multi-shell nanocables have been formed employing various methods to deposit concentric shells. Zhang and Dai used a Ge core and deposited concentric shells of germanium nitride and silicon by CVD followed by an Al_2O_3 gate dielectric shell deposited by ALD and finally an Al metal surround gate shell by isotropic magnetron sputter deposition.[11] The heterostructures were then used to form high current surround gate field effect transistors.

Previously the synthesis of core-shell nanowires has been

[a] *Materials and Supercritical Fluids Group, Department of Chemistry and the Tyndall national Institute, University College Cork, Ireland and Centre for Research on Adaptive Nanostructures and Nanodevices (CRANN), Trinity College Dublin, Dublin 2, Ireland. Fax: +353-214-274097; Tel: +353-214-903301; E-mail: j.holmes@ucc.ie*
[b] *Institut für Anorganische Chemie der Technischen Universität Graz, Stremayrgasse 16, A-8010 Graz, Austria.*
[c] *Department of Chemical Engineering, University of Florida, PO Box 116005, Gainesville, FL 32611-6005, USA*

†Electronic Supplementary Information (ESI) available: [details of any supplementary information available should be included here]. See DOI: 10.1039/b000000x/

limited to a two-step growth mechanism whereby the core nanowire is first grown by a method such as CVD and then the reaction conditions and precursors are changed for the synthesis of the shell.[2, 10] Alternatively, a second independent reaction is employed to deposit a shell to a pre-grown nanowire core.[7] Single step routes for the synthesis of core-shell nanowires have been reported by some authors for the synthesis of Si-SiO_x nanowires. Wu *et al* reported the spontaneous growth of Si-SiO_x by the thermal evaporation of $MoSi_2$ rods in the presence of oxidising agents under controlled conditions.[17] Other authors have also produced Si-SiO_x core-shell nanowires by employing high temperature, ≥ 1000 °C, using various catalysis routes.[18, 19] More recently Ge core SiC_xN_y shell nanocables have been synthesised using a chemical vapour deposition method and the single source precursor material $[Ge(N(SiMe_3)_2)_2]$.[8] These nanocables exhibited a single crystalline Ge core with a uniform amorphous SiC_xN_y shell.

In this paper we describe the control of nanowire morphology by using single source precursor materials employing a single step synthetic process and either Ni or Au nanoparticles as seed catalysts. The morphology of the nanocables consists of a single crystalline Ge nanowire core surrounded by an amorphous SiO_x shell. These nanocables have been characterised using XRD, electron microscopy, EDX, Raman and FTIR spectroscopy. In essence this paper demonstrates the possibility of synthesising novel nanomaterials through the controlled design of novel precursor materials and the careful control of reaction conditions.

Experimental

Synthesis

Gold and nickel nanoparticles were prepared using similar methods to those described by Brust *et al* and Murray and co-workers respectively.[20, 21] In both cases the nanoparticles were initially prepared in toluene but were re-suspended in hexane prior to growing the nanowires. Ge core, SiO_x shell nanocables were synthesised from single source precursor materials, $((CH_3)_3Si)_xGe_y$, with varying Si:Ge ratios prepared and characterised as described elsewhere by Fischer *et al*.[22] It should be noted that the precursor with a Si:Ge ratio of 7:1, is of a slightly different form to that given above, specifically $((CH_3)_3Si)_3Si((CH_3)_3Si)_3Ge$). 10 mg of the single source precursor material was placed into 1 mL stainless steel cells with 0.6 mL of hexane containing, either Au- or Ni-nanoparticles, and the cell sealed. A Ge:Au/Ni atomic ratio of 1000:1 was used in all experiments. The cell was heated to 380 or 400 °C for reactions using Au and Ni seeds respectively, reaching temperature within approximately 10 mins, and held at temperature for 2 hours to degrade the precursor material and crystallise the nanocables. The pressure inside the cell was calculated to be approximately 233 and 259 bar for the experiments performed at 380 °C and 400 °C respectively. At the end of the reaction, the cell was removed from the furnace and quenched to room temperature in iced water. The reaction products were filtered and washed

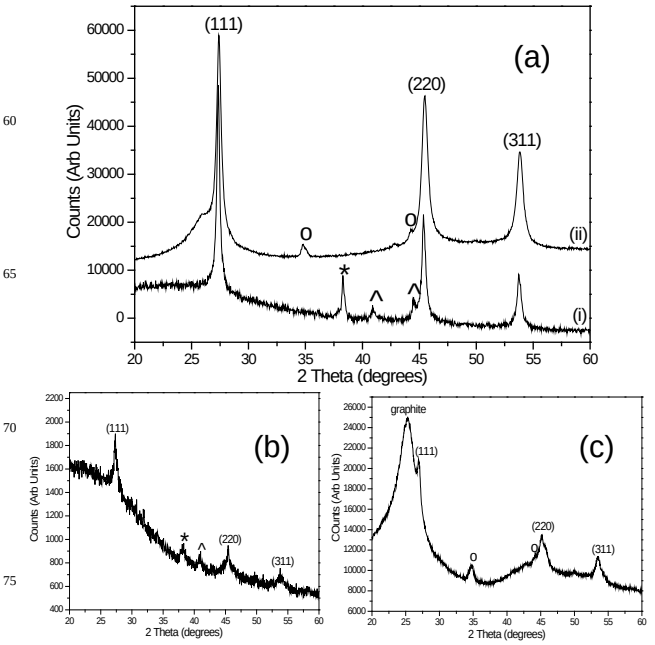

Fig. 1: Typical X-ray diffraction patterns showing the as synthesised SiO_x shell Ge core nanocables exhibiting a highly crystalline Ge structure. (a) grown using the 6:2 Si:Ge precursor material with (i) Au- and (ii) Ni-seed catalysts, (b) shows the poorly crystalline material formed using the 7:1 Si:Ge precursor material with Au-seed catalysts and (c) shows the crystalline material formed using the 7:1 Si:Ge precursor material with Ni-seed catalysts. In the patterns the peaks marked with an * denotes the Au (111) peak attributable to the gold seeds used to catalyse growth, ^ denotes a peaks attributable to a AuGe alloy and o denotes peaks attributable to $NiGe_2$ alloy material formed during the reaction.

with hexane and ethanol and allowed to dry. In an attempt to elucidate the growth mechanism the experiment was also performed under an inert nitrogen atmosphere, whereby, the reaction cell was loaded with 10 mg of the $((CH_3)_3Si)_6Ge_2$ precursor material and 0.6 mL of hexane containing Au- or Ni-nanoparticles and sealed within a nitrogen glovebox. The cell was then removed from the glovebox and heated as described above.

Characterisation

X-ray diffraction data was collected using the Phillips Xpert PW3719 diffractometer using Cu Kα1 radiation (40 kV and 35 mA) over the range $10 \leq 2\theta \leq 60$. A JEOL 2000FX transmission electron microscope (TEM) operating at an acceleration voltage of 200 kV was used for TEM bright and dark field imaging as well as electron diffraction. Energy dispersive x-ray (EDX) analysis was performed using an Oxford Instruments INCA energy system fitted to the TEM. High resolution TEM and scanning TEM images were collected using a JEOL 2010F HRTEM instrument with a STEM attachment operating at an acceleration voltage of 200 kV and the mapping experiments conducted using an Oxford Inca EDS. In all cases, samples were prepared for analysis by sonicating the material in ethanol before a drop of the dispersion was placed on a 400 mesh carbon-coated copper grid for investigation. Raman spectra were collected using the LabRam HR (Horiba Jobin Yvon) Raman system in an ambient atmosphere with a 50 mW NdYAG (λ = 514.5 nm)

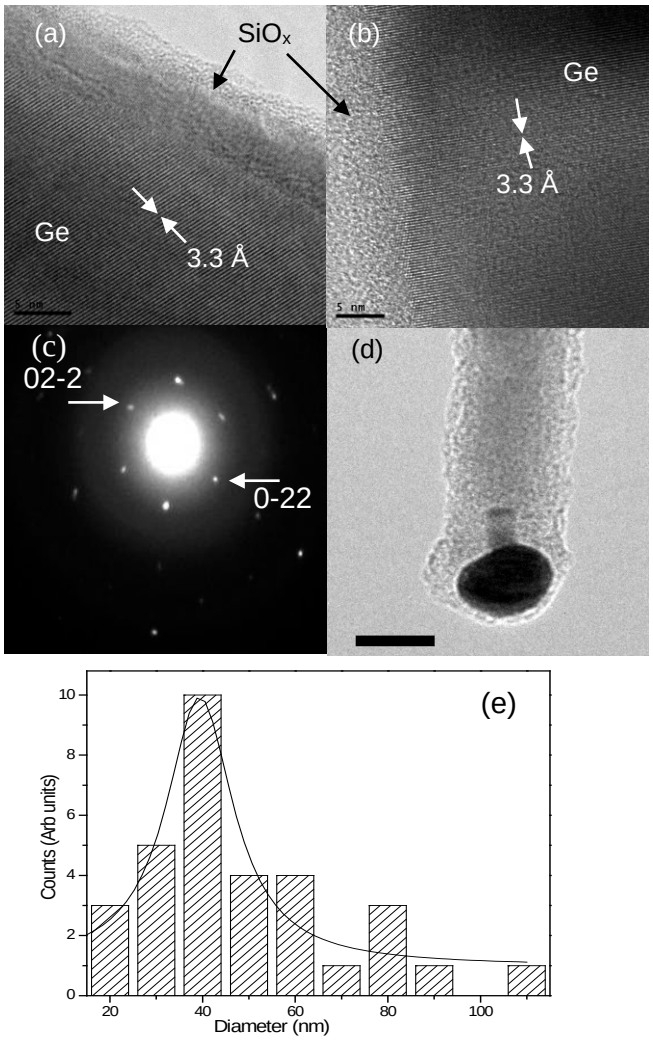

Fig. 2: (a) High resolution transmission microscopy (HRTEM) image showing the amorphous nature of the SiO_x sheath and the single crystalline lattice planes associated with the Ge core of nanocables synthesised from the 6:2 Si:Ge precursor material using Au-seed catalysts. Scale bar represents 5 nm. (b) HRTEM image showing the amorphous nature of the SiO_x sheath and the single crystalline lattice planes associated with the Ge core of nanocables synthesised from the 4:1 Si:Ge precursor material and Au-seed catalysts. Scale bar represents 5 nm. (c) Typical electron diffraction pattern showing the single crystalline nature of these nanocables. (d) High resolution transmission microscopy (HRTEM) image showing the Au tip at the end of these nanocables and the amorphous SiO_x sheath forming around the 'seed' synthesised from the 6:2 Si:Ge precursor material. Scale bar represents 10 nm. (e) Graphical representation of the total nanowire diameter (core + shell) range showing the average nanowire diameter of 40 nm prepared from Au-seed catalysts.

and a CCD detector. Fourier transform infrared (FTIR) spectra were collected at room temperature using a BioRad FTS 3000 instrument. The materials were prepared for analysis using KBr.

Results and Discussion

Typical x-ray diffraction patterns collected for the nanocables synthesised from the $((CH_3)_3Si)_6Ge_2$ precursor material using both Au- and Ni-seed catalysts are shown in Fig. 1. For both

Precursor Composition	Si:Ge Ratio of the precursor	Au-seeded		Ni-seeded	
		d(111)	a (Å)	*d*(111)	a (Å)
$((CH_3)_3Si)_6Ge_2$	6:2	3.2648	5.655	3.2534	5.635
$((CH_3)_3Si)_4Ge$	4:1	3.2606	5.648	3.2509	5.631
$((CH_3)_3Si)_6SiGe$	7:1	3.2595	5.646	3.2427	5.616

Table 1: List of SiGe precursors used, their relative Si:Ge ratio's, d-spacing of the (111) peak as extracted from the XRD patterns and the calculated lattice parameter, a, confirming crystalline Ge.

catalysts the observed peaks can be readily indexed to the (111), (220) and (311) planes typical of the Fd-3m cubic lattice of germanium. No differences in the x-ray diffraction patterns of the nanocables synthesised from different single source precursor materials were evident and in all cases the peaks could be indexed to germanium. However, using a precursor material with a Si:Ge ratio of 7:1 gave a poorly resolved x-ray diffraction pattern with a low signal to noise ratio [Fig. 1(b)] consistent with the small amounts of germanium present in the precursor material. Moreover, whilst the material seeded using a Ni catalyst and the 7:1 Si:Ge precursor showed the same poorly resolved XRD patterns, when compared to the patterns collected using the 6:2 and 4:1 precursor materials, the peaks are far better resolved when compared to the Au-seeded material. In addition, the XRD patterns collected from the Au seeded nanocables also exhibit a small contribution from gold clearly seen as a peak at approximately 38° 2θ whilst a contributions from $NiGe_2$ alloy can be seen (~ 35° 2θ) in those seeded from Ni as a result of the growth mechanism discussed in greater detail later in the paper. The lattice parameter, a, for all the nanocable samples was calculated from the relationship between d-spacing and the miller indices using the (111) peak position as given in table 1 for both the Au- and Ni-seeded nanocables. All of the values obtained for the nanocables grown using Au are typical of the lattice parameters of the Ge lattice with no evidence for lattice contraction suggesting there is no formation of a mixed $Ge_{1-x}Si_x$ lattice.[23] In contrast the lattice parameters for the Ni-seeded nanocables show a very small decrease (1-2 %) from typical Ge lattice parameters. This small change possibly results from strain induced in the wires as a result of the Ni seeding process or may suggest that the wires contain small amounts of Si either at the interface or in the wires themselves. However, it is impossible to rule out the formation of $Si_{1-x}Ge_x$ at the interface between the Ge core and SiO_x shell. There are also no peaks in any of the XRD patterns from discrete crystalline Si or SiO_2 phases. However, there is a large deviance in the XRD baseline in the form of a hump between 20 and 30° 2θ suggesting a large amorphous contribution to the XRD patterns.

High resolution transmission electron microscopy (TEM)

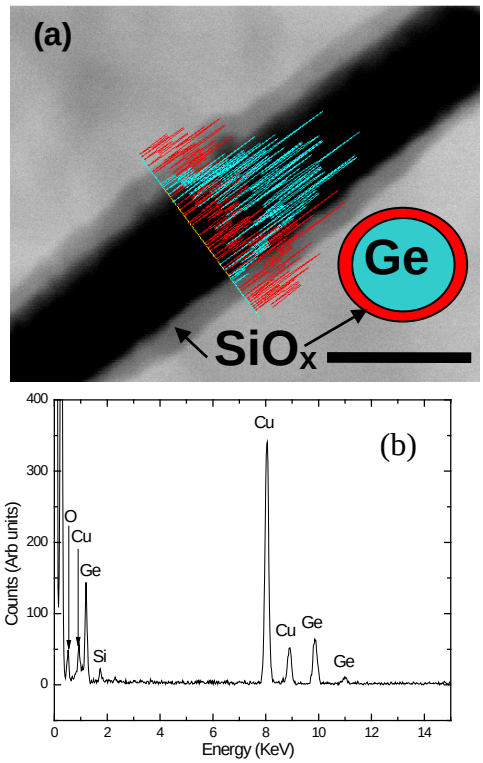

Fig. 3: (a) STEM image of a typical core-shell nanowire showing the regions of Si and Ge mapped onto the nanocable using EDS mapping, where the red line represents the Si and the blue line represents Ge of the nanocables grown using an Au-seed catalyst. Scale bar represents 100 nm. and (b) EDX spectra showing contributions from Si, Ge and O. Note the materials are prepared for TEM analysis on Cu grids resulting in the strong Cu contribution seen in the spectra. Inset of (a) schematic representation depicting the core-shell (Ge-SiO_x) morphology of these nanocables derived from the mapping profile.

images collected for the nanocables synthesised from both the 6:2 and 4:1 Si:Ge precursor materials using Au nanocrystal seeds are given in Fig. 2(a) and 2(b) respectively. These images clearly indicate the core-shell nature of the nanocables and confirm the presence of both a discrete core and shell. It is evident that whilst the Ge appears single crystalline with only one lattice plane evident, there is no crystalline structure associated with the SiO_x shell, which is amorphous. The lattice planes shown in the Ge core are separated by a d-spacing of approximately 3.3 Å attributable to a [111] growth direction. The single crystalline nature is further confirmed by selected area electron diffraction (SAED) with the diffraction pattern attributable to the [111] zone axis of single crystalline Ge also consistent with growth along the [111] direction. SAED patterns were recorded using a diffraction lens of 120 cm and a typical example collected for the nanocables synthesised from the 4:1 Si:Ge precursor, is shown in Fig. 2 (c). Moreover, it can be seen that the shell also forms around the Au seed suggesting that the nanocable core is formed first followed by the deposition of the silica shell [Fig 2(d)]. Measurements collected from a range of nanocables show these materials exhibit total diameters (core + shell) ranging between 15 and 100 nm. However, as shown in Fig. 2(e) the average nanocable diameter is approximately 40 nm with lengths of 100 nm to 500 nm irrespective of the

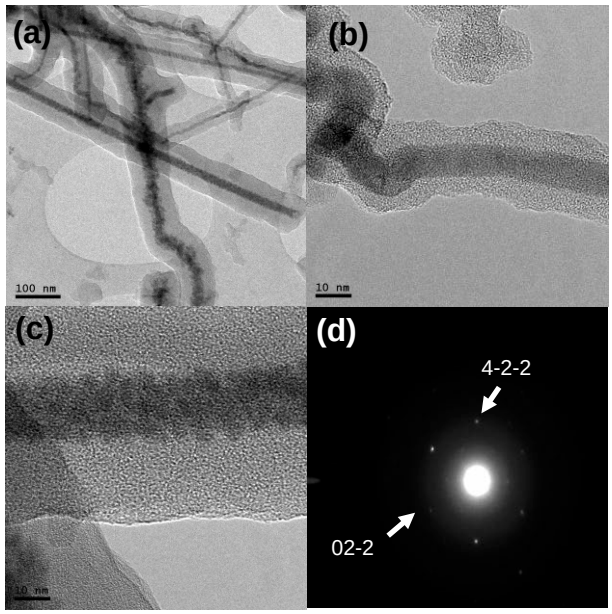

Figure 4: (a) High resolution transmission microscopy (HRTEM) image showing the core-shell nature of the nanocables synthesised from the 4:1 Si:Ge precursor material and a Ni-seed catalyst, scale bar 100 nm, (b) HRTEM image showing the Ni tip at the end of these nanocables and the amorphous SiO_x sheath forming around the 'seed' synthesised from the 6:2 Si:Ge precursor material, scale bar 10 nm, (c) HRTEM image showing the nanocables prepared from the 4:1 Si:Ge precursor material and Ni-seed catalyst showing a defective Ge core which appears to be comprised of smaller nanoparticles, scale bar 10 nm, and (d) Typical electron diffraction pattern showing the single crystalline nature of the smaller diameter non-defective nanocables.

precursor. Furthermore, the SiO_x sheath accounts for approximately 30% of the total nanocable diameter such that the SiO_x wall has an approximate thickness of 6 nm and a 28 nm Ge core for nanocables synthesised from the 4:1 precursor material [Fig. 2]. In all the images studied, the gold seeded nanocables exhibited a Si:Ge ratio of approximately 3:7 independent of both the nanocable dimensions and the Si:Ge ratio of the precursor material used in the synthesis. This result suggests that not all of the available Si in the precursor material is involved in forming the nanocable shell. In comparison with the other (4:1 and 6:2 Si:Ge) precursor materials all reactions undertaken using the 7:1 Si:Ge ratio precursor material resulted in no nanowire growth consistent with the small amount of Ge material available in the precursor to support nanowire growth and observed in the XRD (see supplementary information).

Energy dispersive x-ray (EDX) analysis performed on these nanowires clearly confirms the presence of Si and Ge as well as oxygen, arising from the Ge core and SiO_x shell respectively as shown in Fig. 3. The composition of the nanocables was further investigated using EDS mapping. Fig. 3(a) shows a typical STEM image collected for a nanocable synthesised from the 4:1 precursor material showing an EDS line scan for Si and Ge taken perpendicular to the nanocable growth axis. Fig. 3(b) shows the EDX spectra confirming that Si, Ge, and O are the major constituents of the nanocable. The EDS mapping and EDX spectra clearly show that Ge is confined to the core of the nanocable ruling out the possibility

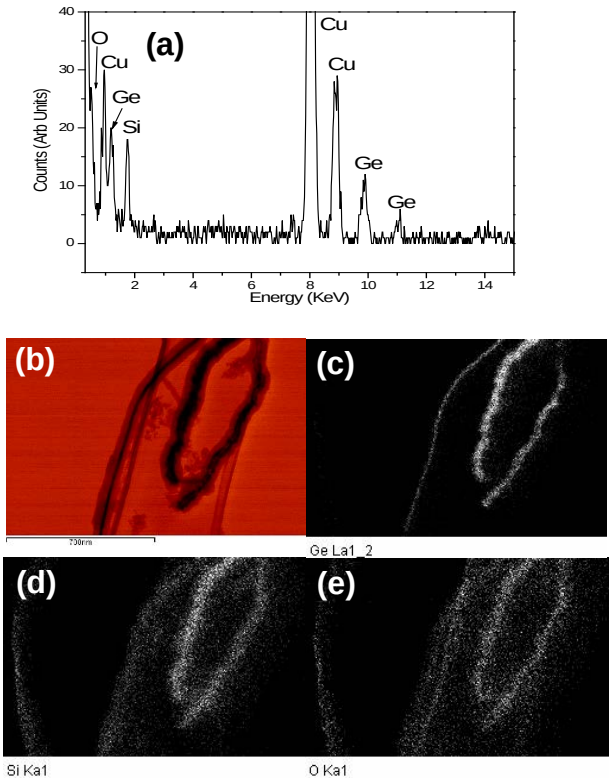

Fig. 5: (a) EDX spectrum collected for the nanocables grown from the 6:2 Si:Ge precursor material and Ni-seed catalysts showing contributions from Si, Ge and O. Note the materials are prepared for TEM analysis on Cu grids resulting in the strong Cu contribution seen in the spectra. (b) STEM bright field image collected for nanocables grown from the 6:2 Si:Ge precursor material and Ni-seed catalysts showing the core-shell morphology, (c) Ge mapping of the image in (b) showing that Ge is confined to the core of the material, (d) Si mapping of the image in (b) and (e) O mapping of the image in (b) confirming that O and Si form the nanocable shell.

that the shell is comprised of GeO_x formed due to oxidation of the Ge nanowires in air. Furthermore, the presence of Si across the whole diameter of the nanocable clearly demonstrates that the shell is comprised of a silicon based material. The inset of Fig. 3(a) shows a schematic model of the core-shell nature of these nanocables as modelled from the EDS map.

In contrast, the nanocables grown using Ni-seed catalysts exhibit much thicker shells than those observed in the Au experiments [Fig. 4]. In all of the images collected both the core and the shell are clearly evident, with the Ni 'seed' visible at the tip of some of these nanocables [Fig. 4(b)]. In contrast with the Au-seeded materials the total nanocable diameter (core + shell) observed is dependent on the Si:Ge precursor material with average total diameters of 40 nm and 60 nm for the 6:2 and 4:1, Si:Ge ratio, precursors respectively. These observations are consistent with those of Tuan and co-workers on Ni-seeded Ge nanowires grown in supercritical toluene.[24] The Ge core dimensions in these nanocables are independent of the precursor material with 80 % of the nanowires investigated exhibiting core diameters less than 15 nm with the majority of these exhibiting diameters less than 10 nm. The difference in the total nanocable diameter

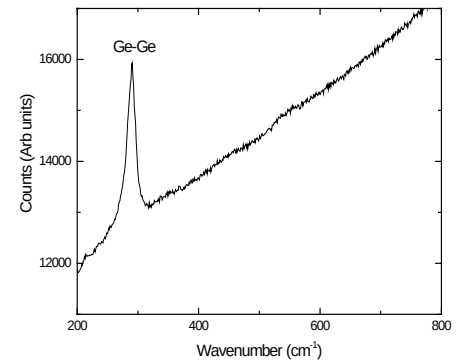

Fig. 6: Typical Raman spectrum of the Ge, Si core, shell nanowire indicating the Ge-Ge interactions at approximately 297 cm^{-1} arising from the Ge core in the Au-seeded nanocables.

observed when using the 6:2 and 4:1 precursors, thus arises from differences in the shell thicknesses which can be seen in the majority of nanocables measured to mirror the Ge:Si ratio of the precursor material suggesting that unlike the nanocables seeded from Au, all the Si is involved in the formation the silica shell. Furthermore, whilst many of these nanocables showed well defined core nanowires some HRTEM images showed poorly formed highly defective cores, with some that appear to be comprised of nanoparticles which coalesced together to form nanowire type structures. These defective cores are subsequently surrounded by a shell to form core-shell nanocables as shown in Fig. 4(c). Close inspection of the TEM images collected show that these defects are limited to the larger core diameter nanowires (> 20 nm) as a result of the seeding mechanism consistent with the results published by Tuan et al. for Ni-seeded Ge nanowires.[24] Due to the thicker nature of the shell observed with Ni seeds it was difficult to see the lattice planes associated with the single crystalline Ge core as the shell scatters incident electrons giving a less resolved image of the core. However, SAED patterns clearly show the single crystalline nature of the core with a typical example shown in Fig. 4 (d). Furthermore indexing of the diffraction pattern shows the [111] zone axis of single crystalline Ge suggesting that the nanowire growth occurs along the [111] direction consistent with the nanocables synthesised using Au-seeds.

Energy dispersive x-ray (EDX) analysis performed on the Ni 'seeded' nanocables clearly confirms the presence of Si, Ge and O as shown in Fig. 5. In comparison with the Au-seeeded nanocables a much stronger contribution from Si can be seen as a result of the formation of much thicker silica shells when using Ni as the seed catalyst. A typical bright field image collected for nanocables grown from the 6:2 precursor material and Ni-seeds using scanning transmission electron microscopy (STEM) is also shown in Fig. 5 with the differences between the core and shell clearly evident further confirming the core-shell motif. Mapping of these nanowires clearly illustrates that Ge is confined to the core of the material, whilst Si and O appear to cover the entire nanocable suggesting that the shell is comprised of silica (Fig. 5) as was observed above for the nanocables synthesised using Au-seed crystals.

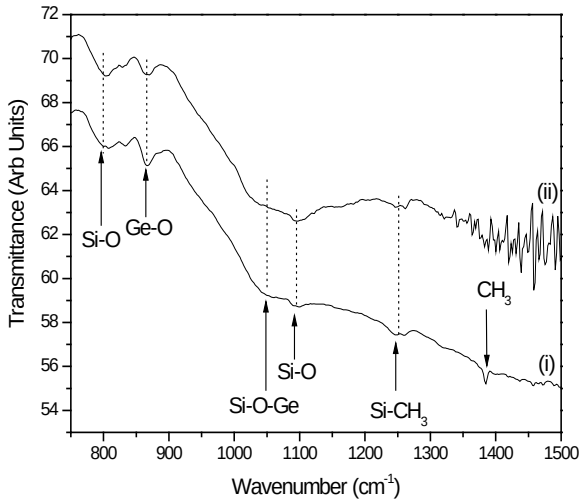

Fig. 7: Typical FTIR spectra showing vibration modes attributed to Si – O, Ge – O and Si – O – Ge interactions confirming the presence of a silica shell for nanocables grown from (i) Au-seed catalysts and (ii) Ni-seed catalysts. In addition vibrations arising from $Si-CH_3$ and CH_3 moieties can be seen in the Au-seeded spectra.

Raman spectroscopy collected for the Au-seeded nanocables, shown in Fig. 6, indicates the presence of Ge-Ge interactions at approximately 297 cm^{-1} in these materials, confirming the presence of a crystalline Ge core. There is no evidence of any Si-Ge or Si-Si interactions at approximately 400 cm^{-1} or 500 cm^{-1} respectively suggesting that a $Si_{1-x}Ge_x$ alloy has not been formed consistent with the XRD observations. Moreover, the lack of Si-Si interactions also confirms that the shell is not comprised solely of Si. Zhang *et al*. have demonstrated previously for Ge nanowires with a GeO_x shell that Raman can be used not only to investigate the Ge-Ge interactions but that valuable information can be gathered from the peak broadening and asymmetry.[25] It can be seen from the Raman spectrum that some degree of peak broadening (FWHM of ~15 cm^{-1}) is observed consistent with Raman studies presented previously for Ge nanowires and core-shell Ge-GeO_2 nanocables.[25, 26] This broadening can possibly be attributed to the influence of strain caused by dimensional confinement.[26] In addition there is also a small degree of asymmetry associated with the peak similar to that observed for the core-shell Ge-GeO_2 nanocables synthesised by Zhang *et al*. Researchers have conflicting views on the nature of this asymmetry, attributing it to confinement effects [25] or an amorphous Ge sheath.[26] Whilst it can be expected that Raman spectra collected for the Ni-seeded nanocables would show the same trends it was not possible to collect this data as a result of the large amorphous contribution arising from the significantly thicker shells effectively 'washing' out the Ge-Ge signal.

Fig. 7 shows typical FTIR spectra collected for both Au- and Ni-seeded nanocables respectively. Both spectra clearly show absorption bands at 803 $cm^{-1}$and 1100 cm^{-1} which can be attributed to stretching vibration modes associated with SiO_2 consistent with the vibration modes previously reported for SiGe and SiO_2 films.[27, 28] In addition there are vibrations at approximately 870 cm^{-1} and 1023 cm^{-1} which can be assigned to Ge-O and Si-O-Ge, respectively.[27] These vibrations can be attributed to the oxygen interface between the silica shell and the germanium core. Furthermore in the Au-seeded nanocables there are also weak modes attributable to C-H stretching modes from $Si-CH_3$ and C-H deformation modes from CH_3 moieties at 1250 cm^{-1} and 1380 cm^{-1} respectively. Since the samples were measured from KBr pellets comprised of the material recovered from the reaction and not solely on a sample comprised of nanocables it is difficult to make a true assignment of the shell material. However, it is possible that the $Si-CH_3$ and CH_3 vibration modes arise from non-nanocrystalline material present in the samples. It is worth noting however that in the Ni-seeded nanocables this contribution is much weaker in comparison with the spectra collected from the Au-seeded nanocables possibly suggesting that in the Ni-seeds result in a more complete decomposition of the precursor material which may be consistent with the formation of thicker shells in these nanocables.

If we first consider the nanocables seeded from Au nanoparticles, the mechanism of seeded growth occurs by atoms dissolving in a nanocrystal (e.g., Au) until it reaches a point of supersaturation resulting in the Ge being expelled as a crystalline wire.[29] Both Si and Ge have similar eutectics with Au ($T(Au:Si)_{eutectic}$ = 361 °C and $T(Au:Ge)_{eutectic}$ = 360 °C) enabling the growth of $Si_{1-x}Ge_x$ nanowires through the Au-catalysed chemical vapour and VLS synthetic methods.[23, 30, 31] Assuming that the single source precursor used in this study fully decomposes prior to nanowire growth, it would be expected that both Si and Ge would supersaturate the Au nanocrystal resulting in the growth of $Si_{1-x}Ge_x$ nanowires with a Si:Ge ratio similar to that of the precursor material. However, the results of this study suggest a two-step mechanism. The first step has Ge dissolving in the Au nanoparticle resulting in the growth of the Ge core nanowire. This step is supported by the fact that the Ge core diameter is strongly correlated to the Au nanoparticle diameter. Cui *et al* have shown that the diameter of the VLS nanowires depends on the seed diameter.[32] In the Ge starved reactions with the Si:Ge 7:1 precursor, EDX shows only the Ge dissolved in the Au nanoparticles. These systems lack sufficient Ge concentrations to saturate the nanoparticle and initiate nanowire formation. The second step involves subsequent deposition of the Si as an amorphous silica shell. Although the exact mechanism is not clear, it appears that the presence of water and/or oxygen may play a role in the amorphous silica layer (discussed further below).

In contrast the Ni-Si and Ni-Ge phase diagrams are far more complex with the lowest temperature eutectics > 750 °C. These temperatures are far in excess of the temperatures employed in these experiments suggesting that the nanocables no longer form by aVLS growth method as described above for the Au-catalysed nanocables. Tuan *et al* have previously demonstrated the growth of both Si and Ge nanowires from Ni nanoparticles by a solid-phase seeding mechanism from the formation of solid alloys below 500 °C and it can be suggested that the Ge core forms by this method.[24, 33, 34] Moreover, it can be seen Ni-seed crystals result in nanocables with very similar

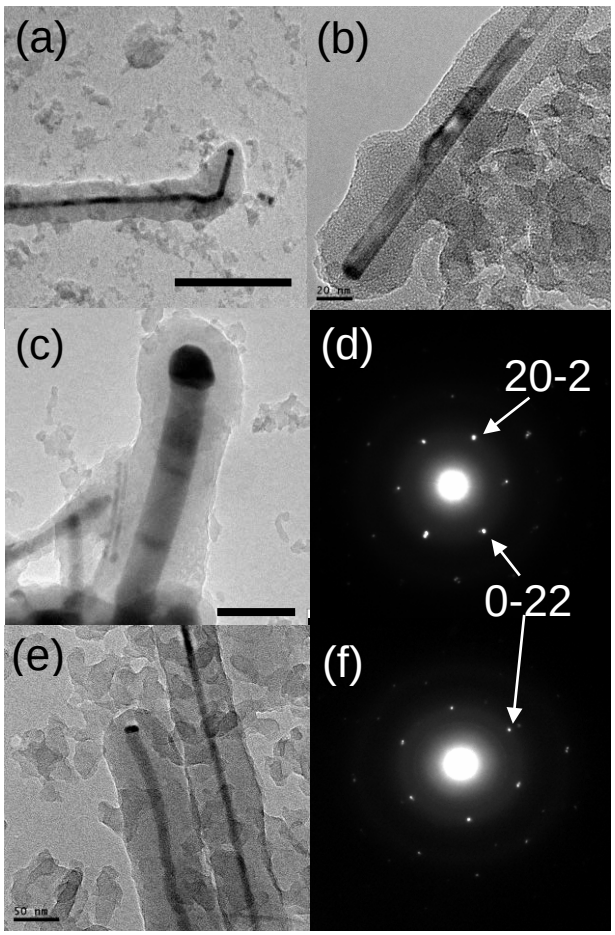

Fig. 8: (a) and (b) TEM images, showing the morphology of the nanocables grown in an inert atmosphere with a Au-seed catalyst. The thicker SiO_x shell is clearly evident around the Ge core. Scale bar represents 500 nm and 20 nm in image (a) and (b) respectively, (d) and (f) Typical selected area electron diffraction patterns showing the single crystalline nature of these nanocables. (c) and (e) TEM images, showing the morphology of the nanocables grown in an inert atmosphere with a Ni-seed catalyst. Scale bar represents 100 nm and 50 nm in image (c) and (e) respectively. In both cases these nanocables were synthesised from the 6:2 Si:Ge precursor material.

morphologies to those obtained using Au seeds (i.e. crystalline Ge core coated with an amorphous silica shell) suggesting again that the Ge nanowires seed first followed by the deposition of the silica shell further supporting the suggestion of a two step growth mechanism.

This two-step mechanism suggests a complex decomposition of the precursor. Tuan *et al*. have reported the synthesis of silicon nanowires using nickel nanocrystals as seeds.[33] During their investigations, attempts to seed crystalline silicon nanowires from Au nanocrystals in sc-hexane using alkylsilane precursors were unsuccessful. They concluded that Au nanocrystals did not catalyse the decomposition of the alkylsilane. In a similar manner, the Si-C bond of our precursor will not undergo thermolysis at low temperatures. In addition, the alkyl moiety is not as kinetically labile as the phenyl group in diphenyl silane, which readily disproportionates to form silane.[29, 31, 33] Further support for this two step mechanism is observed in experiments done at higher temperatures (≥ 500 ^oC). The faster decomposition kinetics at higher temperatures should yield more Si atoms. Once again, these systems yielded core-shell structures rather than $Si_{1-x}Ge_x$ nanowires with the same core/shell ratios and nanowire morphologies as low temperature reactions. This insensitivity to temperature suggests that Si does not play a major role in the first step of the mechanism. Mathur and co-workers proposed that the morphology of Ge-SiC_xN_y, core-shell nanocables was formed as a result of the preferential decomposition of the single source precursor material such that Ge is liberated from the precursor first.[8] These results are consistent with the Ge-Si bond enthalpy of 301 $kJmol^{-1}$ which requires considerably less energy to cleave than the Si-C bond enthalpy of 451.4 $kJmol^{-1}$.[35]

In contrast to the nanocables formed by Mathur *et al.* [8] when using Au-seed catalysts it is clear that not all the available Si in the precursor material is involved in the formation of the shell suggesting that a more complex mechanism after preferential decomposition of the precursor material is prevalent or possibly suggests that the precursor does not fully decompose to yield all the available Si. Moreover the formation of core-shell ratios that more accurately mirror the Si:Ge ratio of the precursor material when using Ni-seed catalysts suggests that the Ni plays a more active role in precursor decomposition when compared with Au consistent with the observations of Tuan *et al*.[33] In an attempt to elucidate the growth mechanism fully, reaction vessels were sealed in a nitrogen atmosphere rather than air using the 6:2 Si:Ge precursor and the same source of Au-nanoparticles or Ni-nanoparticles in hexane as the previous reactions. TEM images of these materials clearly showed that the core-shell morphology of these nanocables was maintained in the absence of air with both Au- and Ni-seed catalysts [Fig. 8].

In contrast to the materials prepared in air using Au-seed crystals, the nanocables formed in nitrogen exhibited larger average total diameters (core + shell) of approximately 60 nm as a result of the formation of thicker silica shells. Measurements of the shell and core dimensions indicates that at least 80% of all nanocables exhibit shell:core ratios that reflect the Si:Ge ratio of the precursor material. No observable differences between the product formed in either air or nitrogen with Ni as a seed catalyst was evident with the same core-shell morphologies that mirror the Si:Ge ratio of the precursor material observed as shown in Fig. 8. In both cases the lattice planes associated with the single crystalline Ge cores are not evident in these images due to the thick nature of the shell obscuring the lattice planes. The single crystalline nature of the Ge core can, however, be confirmed by SAED which clearly shows diffraction spots associated with the [111] zone axis and a [111] growth direction identical to the materials prepared in air [Fig. 8].

The initial results seem to support the idea that Ni contributes to the decomposition of the precursor material whilst Au does not, consistent with the initial reports that Au does not produce Si nanowires from alkyl silane precursor

materials.[33] However, this is not supported by the data collected in the absence of air where a full shell is deposited onto the nanowires when using Au-seed crystals confirming that the precursor materials are fully decomposing. This suggests that oxygen and/or water molecules play a role, perhaps forming a liquid or gaseous by-product formed by reacting with trimethylsilyl groups released once germanium is liberated from the precursor. We have already argued that Ge nanowires form first due to differences in the decomposition kinetics. We further note that Ge nanowires are needed for silica growth/decomposition. In the germanium starved conditions of the 7:1 Si:Ge precursor, there is insufficient Ge to reach supersaturation in the Au nanocrystals and no germanium nanowires form.

Tuan et al have recently demonstrated the growth of amorphous silica nanotubes and nanofibres from CuS and Au nanoparticles via solid-phase seeding and SFLS growth mechanisms respectively.[36] They showed that whilst Si nanowires were formed in the absence of water and oxygen, amorphous silica nanotubes and nanofibres formed when oxygen and water were present. Increasing the amount of water and/or oxygen in the reaction exhibited a marked difference in the quality of the nanotubes produced. At low water contents good quality silica nanotubes were formed. However, increasing the water content resulted in lower yields and nanotubes with roughened silica walls as well as increasing yields of particulates. At very high water contents the authors observed no nanotube formation with only amorphous silica particulates formed. They concluded that whilst oxygen and water are needed for the formation of the silica, oxidation of the silica precursor in the bulk of the reactor volume occurs which competes with nanotube formation.[36]

Conclusions

We report here the synthesis of Ge-SiO_x, core-shell nanowires grown via SFLS and supercritical fluid-solid-solid (SFSS) mechanisms using a single step supercritical fluid method. These materials are comprised of a single crystalline Ge core coated with an amorphous SiO_x sheath, as confirmed by XRD, TEM, FTIR and Raman spectroscopy. Semiconductor heterostructured nanowires offer a platform for the design of multifunctional devices compatible with current CMOS technology and thus the ability to carry out a synthesis in a single step process is advantageous, offering many benefits over multi-step processes, such as reduced running costs and higher yields. We have demonstrated here that careful design of precursor materials in combination with controlled reaction conditions can lead to the synthesis of nanomaterials with specific morphologies.

Acknowledgements

We acknowledge financial support from Science Foundation Ireland (Grant 07/RFP/MASF710). We are grateful to Siebein and the UF Major Analytical Instrumentation Centre, Peter Nellist and Galvin Behan for assistance with high resolution imaging and analysis. Thanks also to Joseph Tobin and Gary Attard for Raman analysis.

References

1 J. L. Gong, Y. Liang, Y. Huang, J. W. Chen, J. H. Jiang, G. L. Shen, R. Q. Yu, *Biosensors and Bioelectronics*, 2007, **22**, 1501.
2 L. J. Lauhon, M. S. Gudiksen, D. Wang, C. M. Lieber, *Nature*, 2002, **420**, 57.
3 B. Daly, D. C. Arnold, J. S. Kulkarni, O. Kazakova, M. T. Shaw, S. Nikitenko, D. Erts, M. A. Morris, J. D. Holmes, *Small*, 2006, **2**, 1299.
4 T. A. Crowley, B. Daly, M. A. Morris, O. Kazakova, D. Erts, J. J. Boland, B. Wu, J. D. Holmes, *J. Mater. Chem.*, 2005, **15**, 2408.
5 B. Daly, J. S. Kulkarni, D. C. Arnold, M. T. Shaw, S. Nikitenko, M. A. Morris, J. D. Holmes, *J. Mater. Chem.*, 2006, **16**, 3861.
6 O. Hayden, A. B. Greytak, D. C. Bell, *Adv. Mater.*, 2005, **17**, 701.
7 S. Han, D. Zhang, C. Zhou, *Appl. Phys. Lett.*, 2006, **88**, 133109.
8 S. Mathur, H. Shen, N. Donia, T. Rugamer, V. Sivakov, U. Werner, *J. Am. Chem. Soc.*, 2007, **129**, 9746.
9 D. Bodlaki, H. Yamamoto, D. H. Waldeck, E. Borguet, *Surface Science*, 2003, **543**, 63.
10 J. Xiang, W. Lu, Y. Hu, Y. Wu, H. Yan, C. M. Lieber, *Nature*, 2006, **441**, 489-493.
11 L. Zhang, R. Tu, H. Dai, *Nano Lett.*, 2006, **6**, 2785.
12 B. V. Kamenev, J. M. Baribeau, D. J. Lockwood, L. Tsybeskov, *Physica E.*, 2005, **26**, 174.
13 C. Y. Ko, W. T. Lin, *Nanotechnology*, 2006, **17**, 4464.
14 B. V. Kamenev, L. Tsybeskov, J. M. Baribeau, D. J. Lockwood, *App. Phys. Lett.*, 2004, **84**, 1293.
15 A. Javey, S. Nam, R. S. Friedman, H. Yan, C. M. Lieber, *Nano Lett.* 2007, **7**, 773.
16 J. Xiang, A. Vidan, M. Tinkham, R. M. Westervelt, C. M. Lieber, *Nature Nanotechnology*, 2006, **1**, 208.
17 C. Wu, W. Qin, G. Qin, ., D. Zhao, J. Zhang, W. Xu, H. Lin, *Chem. Phys. Lett.*, 2003, **378**, 368.
18 B. T. Park, K. Yong, *Nanotechnology*, 2004, **15**, S365-S370.
19 H. Wang, X. Zhang, X. Meng, S. Zhou, S. Wu, W. Shi, S. Lee, *Angew. Chem. Int. Ed.*, 2005, **44**, 6934-6937.
20 M. Brust, M. Walker, D. Bethell, D. J. Schriffin, R. J. Whyman, *J. Chem. Soc. Chem. Commun.*, 1994, **7**, 801.
21 C. B. Murray, S. Sun, H. Doyle, T. Betley, *MRS Bull.*, 2001, **26**, 985.
22 J. Fischer, J. Baumgartner, C. Marschner, *Organometallics*, 2005, **24**, 1263.
23 J. E. Yang, C. B. Jin, C. J. Kim, M. H. Jo, *Nano Lett.*, 2006, **6**, 2679.
24 H-Y. Tuan, D. C. Lee, T. Hanrath, B. A. Korgel, *Chem. Mater.*, 2005, **17**, 5705.
25 Y. F. Zhang, Y. H. Tang, N. Wang, C. S. Lee, I. Bello, S. T. Lee, *Phys. Rev. B*, 2000, **61**, 4518.
26 S. Mathur, H. Shen, V. Sivakov, U. Werner, *Chem. Mater.*, 2004, **16**, 2449.
27 A. King, J. C. Soares, A. C. Prieto, J. Jimenez, A. Rodriguez, J. Sangrador, T. Rodriguez, *Nucl. Inst. and Meth. in Phys. Res. B*,. 2005, **240**, 405.
28 H. Gerung, C. J. Brinker, S. R. J. Bruek, S. M. Han, *J. Vac. Sci. Technol. A.*, 2005, **23**, 347.
29 J. D. Holmes, K. P. Johnston, R. C. Doty, B. A. Korgel, *Science*, 2000, **287**, 1471.
30 K. K. Lew, L. Pan, E. C. Dickey, J. M. Redwing, *J. Mater. Res.*, 2006, **21**, 2876.
31 T. Hanrath, B. A. Korgel, *Adv. Mater.*, 2003, **15**, 437.
32 Y. Ci, L. J. Lauhon, M. S. Guddiksen, J. Wang, C. M. Lieber, *App. Phys. Lett.* 2001, **78**, 2214.
33 H.-Y. Tuan, D. C. Lee, T. Hanrath, B. A. Korgel, *Nano Lett.*, 2005, **5**, 681.
34 H.-Y. Tuan, D. C. Lee, B. A. Korgel, *Angew. Chem. Int. Ed.*, 2006, **45**, 5184.
35 "Molecular Structure and Spectroscopy", in *CRC Handbook of Chemistry and Physics, Internet Version 2005*, David R. Lide, ed, <http://www.hbcpnetbase.com>, CRC Press, Boca Raton, FL, 2005.
36 H.-Y. Tuan, A. Ghezelbash, B. A. Korgel, *Chem. Mater.*, 2008, **20**, 2306.